Novel non-linear control for synchronization and power sharing in islanded and grid-connected mesh microgrids

Youssef Hennane, Abdelmajid Berdai, Serge Pierfederici, Farid Meibody-Tabar, Jean-Philippe Martin

Novel Non-linear Control for Synchronization and Power Sharing in Islanded and Grid-connected Mesh Microgrids

Youssef Hennane[a,b,*], Abdelmajid Berdai[b], Serge Pierfederici[a], Farid Meibody-Tabar[a], Jean-Philippe Martin[a]

[a]*Université de Lorraine, CNRS, LEMTA, Nancy F-54000, France*
[b]*Energy and Electrical Systems Laboratory National School of Electricity and Mechanics, ENSEM, University Hassan II of Casablanca Casablanca, Morocco*

Abstract

In this paper, a novel distributed nonlinear control strategy of mesh microgrids' distributed generators (DGs) based on droop control approaches is proposed. It ensures secure synchronization of DGs and their accurate active and reactive power sharing in both islanded and grid-connected operating modes of mesh microgrids. This control method allows also a seamless transition from islanded to grid-connected modes without affecting the DGs' active and reactive power sharing during synchronization as well as controlling independently the exchanged active and reactive powers with the main grid. The efficiency of the proposed control strategies is verified first by Simulink/Simscape simulation results and then validated by experimentations using Hardware-in-the-Loop (HIL) real time simulator of opal-rt and dSPACE platforms. The control robustness is also investigated with respect to the load variation, the microgrid topology modification and the communication time delays.

Keywords: Distributed Generators, Droop control, HIL simulation, Mesh Microgrids, Power sharing, Synchronization

1. Introduction

Microgrids powered by clean renewable energy sources via controllable power converters allow a fast-dynamic response to sudden load variations and thus reduce the risk of its instability. Mesh-type microgrids can provide higher power availability than microgrids with simple architectures where DGs are connected to a single common coupling point [1]. However, most renewable energy sources are intermittent and can't continuously supply the loads connected to islanded microgrids. To reduce the size and cost of microgrid storage units, attenuating the severity of the aforementioned problem, microgrids should have the ability to operate in grid-connected mode [2]-[3]. In island and grid-connected microgrid operating modes, the load power should be shared by the DG units in proportion to their power ratings or available powers [4], which can avoid overstressing and delay aging of the sources. The active power-frequency (P-ω) and reactive power-voltage (Q-V) droop control method is the most used approach to achieve accurate power sharing in microgrids [4]-[8]. Due to the active and reactive power coupling phenomenon, caused by microgrids' power line impedances, power sharing between the DGs, in particular reactive power sharing, is difficult

* Corresponding author. Tel.: +33-7-53-06-75-73.
E-mail address: youssefhennane@gmail.com

to achieve using conventional droop control strategies [9]-[10]. To address the problem of inaccurate reactive power sharing in microgrids, the authors of [11] proposed a modified double-loop voltage controller without using droop control method. However, when a communication failure occurs, the supply of the power loads is interrupted. In [12] authors proposed an optimal angle droop for reactive power sharing enhancement by employing one-loop flatness-based control to perfectly control the output voltage of inverters with smaller THD and high bandwidth. While in [13], the authors proposed to compensate the line impedance mismatches by controlling the reactive power in proportion to the derivative of the DG's output voltage. However, all strategies in [11], [12] and [13] are developed for mono-PCC microgrids and cannot guarantee an accurate reactive power sharing in mesh microgrids. The variable structure of meshed microgrids makes it challenging to achieve accurate reactive power sharing due to the difficulty of detecting line impedance mismatches [1], [14], [15].

The active and reactive power sharing in droop-controlled islanded mesh microgrids with multiple-PCC are the subject of a certain number of research works. In [1], the authors use an adaptive regulation of the virtual impedances to achieve an accurate active and reactive power sharing without any knowledge of the detailed configuration of the microgrid. Despite of allowing the plug and play functionality, the proposed controller is centralized and requires a high-speed two-way communication system to collect the massive amount of informations from all DGs, which must then be processed using a very powerful calculator. As a result, any failure in the centralized controller may cause the system to stop working. In [16], the authors propose a virtual impedance optimization method for reactive power sharing in mesh microgrids. But the robustness of this reactive power sharing method is not verified or discussed with respect to the modification of considered mesh microgrid topology. In [17], the authors propose a modified droop-control strategy to ensure active and reactive power sharing between DGs in a mesh microgrid by adding a nonlinear coefficient. In addition, this control strategy, verified only by simulation results, ensures DGs' accurate active and reactive power sharing. But, the robustness of this control method is not verified or discussed with respect to the topology modifications of the considered mesh microgrid. However, the efficiency of the proposed control strategies in [1], [16]-and [17] is verified only in islanded mesh microgrids and their grid connected operating mode is not studied.

In grid-connected operating mode of a mesh microgrid, the first challenge is its synchronization and connection as a unit to the main grid without affecting the active and reactive power sharing [18]-[19]. The second challenge is to control independently the exchanged active and reactive powers with the main grid [20]. In [19], authors propose a synchronization method based on droop control. The method is based on centralized PI controller and ensures a seamless transition from islanded to grid-connected operating mode of microgrids without affecting DGs' active power sharing. But the authors did not discuss the effect of the synchronization on the reactive power sharing of DGs. The authors in [21] propose a power sharing method for a grid-connected Microgrid with Multiple Distributed Generators. They present a coordinated control method for inverter-based DGs so that the microgrid is always regulated as a controllable load from the utility point of view in grid-connected mode, and the frequency deviation in the transition mode is minimized. Although the proposed method allows the considered microgrid a seamless transition from islanded to grid-connected mode and ensures the active power sharing of DGs, the reactive power sharing is not considered.

Motivated by the mentioned work, the nonlinear control strategy in [17], proposed for active and reactive power sharing of DGs in only islanded microgrids, is improved to additionally ensure synchronization of DGs and their accurate power sharing in both islanded and grid-connected operation modes. Furthermore, this control ensures a smooth transition between the operating modes of the mesh microgrids without affecting the power sharing of the DGs. In addition, the active and reactive powers exchanged with the main grid in grid-connected mode are imposed independently. For both operating modes of the mesh microgrids, the robustness of the proposed control strategy with respect to large load variations, modifications of the microgrid topology and communication delays is also investigated.

To present the proposed control strategy and prove its efficiency and robustness in both operating modes, the paper is organized in 5 sections.

In section 2, a first case study is discussed in order to apply the control method proposed in [17], for DGs' synchronization and power sharing in islanded mesh microgrids having a higher number of DGs (3 DGs compared to

2 DGs in [17]) and also to validate its efficiency by experiments using Hardware-in-the-Loop (HIL). In addition, the robustness of the proposed control with respect to microgrid topology modifications is investigated. For this purpose, a 3-DG mesh microgrid is considered. For this case, to show the plug and play feature, DGs and loads are connected to the microgrid at random instants. Also, to show the robustness of the proposed control with respect to the microgrid topology modifications and the load variations, different loads and power lines are randomly disconnected and reconnected.

In Section 3, the proposed nonlinear control in [17] is improved and adapted to provide a seamless transition from islanded to grid-connected mode, without affecting DGs' active and reactive power sharing. For this purpose, a second case study concerning a 2-DG mesh microgrid with the possibility of connection to the main grid is considered. For microgrids with the ability to operate in grid-connected mode, the node through which the microgrid can be connected to the main grid is chosen as the pilot node; the information on its voltage vector is used not only for synchronization of the microgrid with the main grid, but also for ensuring DGs' power sharing in both islanded and grid-connected modes. It should be noted that, the proposed nonlinear control method allows also to impose the exchanged active and reactive powers with the main grid, without affecting the power sharing of microgrid DGs. In addition, the robustness of the microgrid control in grid-connected mode is also investigated when some loads or DGs are suddenly connected or disconnected or when the microgrid topology changes due to sudden power lines disconnection or reconnection. The simulation results using Simscape and experimental results using real-time HIL simulations confirm the effectiveness of the proposed control for allowing seamless transition from islanded mode to grid connected one of mesh microgrids as well as ensuring accurate DGs' active and reactive power sharing in both microgrid operating modes, even when its topology is dynamically modified.

The proposed control is distributed and uses information on the RMS voltage value measured at a pilot node which is sent to all DGs in the microgrid creating a low-speed one-way communication in the microgrid. Therefore, in section 4 the impact of communication delay on the proposed control is examined and evaluated by conducting several tests considering various time delays [22]-[23]. The maximum delay that doesn't affect the microgrid stability is determined via MATLAB/Simulink simulations. For this case study, the 3-DG mesh microgrid used in section 2 is considered to show the impact of communication time delays on the microgrid stability. The last section is devoted to the synthesis of the most significant results and conclusions.

Nomenclature

DG	Distributed generator
HIL	Hardware in loop
PCC	Point of common coupling
Mono-PCC	Single Point of common coupling
Multi-PCC	Multiple Point of common coupling
RMS	Root mean square
RLC	Resistor, inductor and capacitor
µGpcc	The point of common coupling where the microgrid can be connected to the main grid
Mode 1	Islanded operating mode
Mode 2	Grid-connected operating mode
P_{in}, Q_{in}	Rated values of active and reactive powers of the ith DG
P_{fi}, Q_{fi}	Filtered values of the measured active and reactive powers of the ith DG
ω_n, E_n	Rated values of the pulsation and voltage of the microgrid
m_i, n_i	Frequency and voltage droop control coefficients of the ith DG
Δ_ω, Δ_E	Permissible variations of pulsation and voltage.
K_I	Integral factor for determining J_i in (3)
ε_i	Relative error for power sharing of the ith DG, used for determining J_i in (3)
E_{ref}	Measured voltage of the pilot node (µGpcc) of the considered mesh microgrid
ω_i, E_i, ξ_i	The ith DG pulsation, the ith DG voltage module and its phase angle (argument)
$\omega_{pcci}, E_{pcci}, \xi_{pcci}$	The ith PCC pulsation, the ith PCC voltage module and its phase angle (argument)
$S1_i, S2_i$	Integral terms in (6) and (7), used for synchronization of the ith DG to the microgrid
B_i	Binary coefficient that is equal 1 during the synchronization of the ith DG and equal 0

	otherwise, used in (6), (7), (11) and (12)
K_{ai}, K_{bi}	Integral factors for frequency and phase synchronization, used for determining $S1_i$
K_{ci}	Integral factor for voltage synchronization, used for determining $S2_i$
$\omega_{\mu Gpcc}$, $E_{\mu Gpcc}$, $\xi_{\mu Gpcc}$	The µGpcc pulsation, the µGpcc voltage module and its phase angle (argument)
$\omega_{Gridpcc}$, $E_{Gridpcc}$, $\xi_{Gridpcc}$	The main grid pulsation, the main grid voltage module and its phase angle (argument)
$S3_i$, $S4_i$	Integral terms in (11) and (12), used for synchronization of the microgrid to the main grid
P_{exch}	The measured active power at µGpcc, used for controlling the exchanged power with the main grid
$P_{exchref}$	The reference of the exchanged active power with the main grid
$Exch_P$	Integral terms used in (11) for controlling the exchanged active power with the main grid
K_{I1}, K'_{I1}	Integral factors for determining $Exch_P$ and $Exch_Q$
E_{abcref_i}	The ith DG 3-phase voltage reference
E_{abc_i} , I_{abc_i}	The measured values of the ith DG 3-phase voltage and current
E_{dq_i} , I_{dq_i}	The measured values of the ith DG voltage and current in d-q
T_d	Communication delay.

2. Power Sharing and Synchronization Strategies in Mesh Islanded Microgrids

In practical applications, the conventional P-ω droop control method is able to achieve an accurate active power sharing while the frequencies of different DG units in the microgrid converge to the same value close to the microgrid rated frequency [7]-[8]. This method for imposing almost the same frequency to all DGs remains efficient even in the complex mesh-type microgrids. However, the conventional Q-V droop control method to impose the voltages of the microgrid DGs cannot ensure their reactive power sharing, particularly in mesh-type microgrids due to their complex topologies and the impedances of their power lines. In the following, we present first the proposed control method for efficient active and reactive power sharing in multi-PCC mesh islanded microgrids and the adapted synchronization strategy for connecting its DGs in [17]. The simulation results based on a Simscape model of a 3-DG islanded mesh microgrid of Figure 1, instead of the 2-DG mesh-microgrid tested in [17], give a first validation of the proposed control strategies in a more complex microgrid. In addition, an experimental validation approach of these control strategies based on hardware-in-the-loop (HIL) real time tests allows to confirm their efficiency in the case of a 2-DG mesh microgrid of Figure 2. Both microgrids in Figures 1 and 2 are inspired from the IEEE 9 bus test feeder. The different PCCs are interconnected with power lines, modeled by RLC circuits (π-type model). All the microgrid data are presented in tables 1 and 2.

2.1. Power sharing in islanded mesh microgrids

In a single-bus microgrid, all the DG units are connected to the common AC bus through their respective DG's feeders. By comparing the impedance values of these feeders, the reactive power sharing performance of system can be basically obtained. However, for a mesh microgrid, it's not straightforward to evaluate the system reactive power sharing performance as it's not easy to analyse such complex systems due their high number of variables. In mesh microgrids, each line, connecting the ith PCC to the jth one, has a non-negligible inductance ($\boldsymbol{\lambda_{i,j}}$) and resistance ($\boldsymbol{\rho_{i,j}}$), leading to a line voltage drop $\boldsymbol{\Delta E_{i,j}}$ as expressed in equation (1) between these two PCCs that is proportional to the line current $\boldsymbol{I_{i,j}}$ and creates a coupling between the active power ($\boldsymbol{P_{i,j}}$) and reactive power ($\boldsymbol{Q_{i,j}}$) exchanged between ith and jth PCCs.

$$\Delta E_{i,j} = \rho_{i,j} \times I_{i,j} \times cos\,\varphi + \lambda_{i,j} \times \omega I_{i,j} \times sin\,\varphi = \frac{\rho_{i,j} \times P_{i,j} + \lambda_{i,j} \times Q_{i,j}}{E_j} \quad (1)$$

where E_j is the voltage RMS value of the jth PCC.

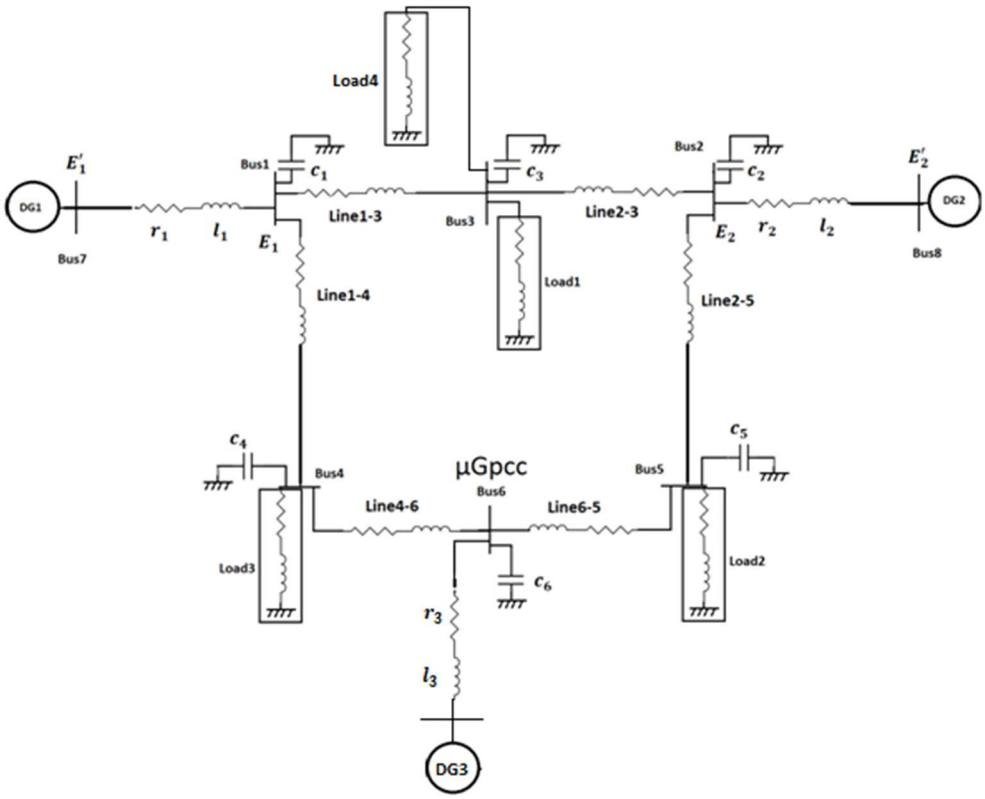

Fig.1. Islanded 3-DGs mesh microgrid

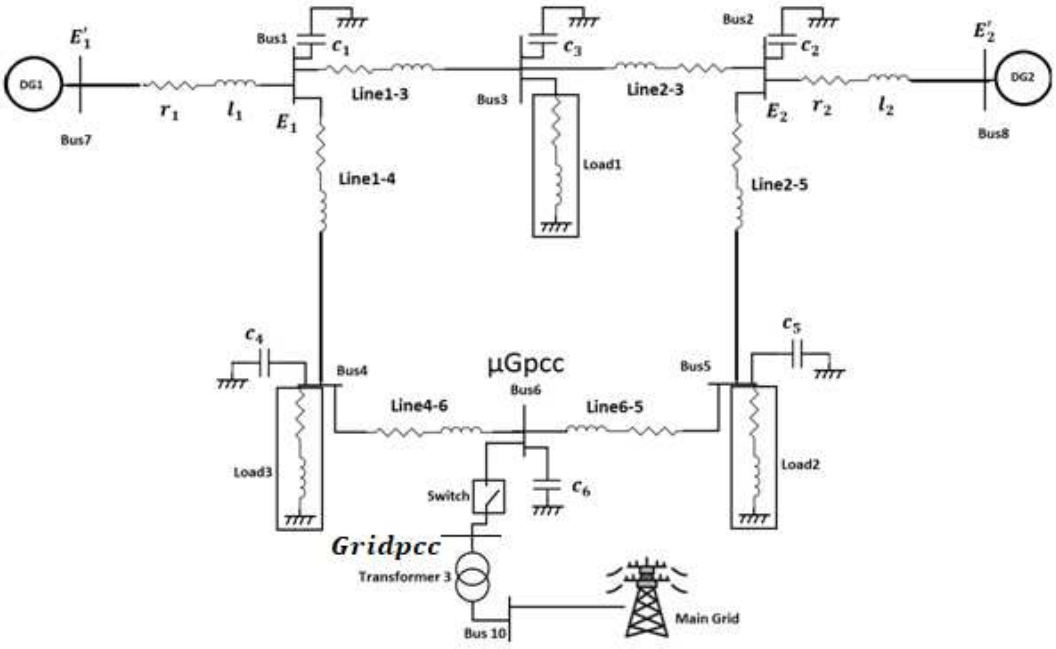

Fig.2. Considered mesh microgrid inspired from IEEE 9 bus test feeder

Table 1. Parameters of the considered microgrid power lines

Lines	Resistance (Ω)	Inductance (mH)	Capacitance (nF)	Points of connections
Line 7-1	0.01	1.14	50	Bus 7- Bus 1
Line 8-2	0.01	1.14	50	Bus 8- Bus 2
Line 1-3	0.629	7.14	50	Bus 1- Bus 3
Line 2-3	0.629	7.14	50	Bus 2- Bus 3
Line 1-4	0.629	8.5	50	Bus 1- Bus 4
Line 2-5	0.629	8.5	50	Bus 2- Bus 5
Line 4-6	0.659	8.7	50	Bus 4- Bus 6
Line 5-6	0.714	8.7	50	Bus 5- Bus 6

Table 2. sources and loads powers

Sources and Loads	Rated Active Power (kW)	Rated Reactive Power (kVAr)	Rated Phase to Phase Voltage (V)	Point Of connection
Source 1	14.5	5.3	400	Bus 1
Source 2	10	4	400	Bus 2
Source 3	7.5	6.3	400	Bus 6
Load 1	5	0.7	400	Bus 3
Load 2	4.5	0.9	400	Bus 5
Load 3	4	1	400	Bus 4
Load 4	7	5.8	400	Bus 3

In order to achieve an efficient active and reactive power-sharing between DGs of microgrids including islanded multi-PCC mesh Microgrids without any knowledge of the microgrid structure, the classical frequency Droop control equation in (2) was not modified but the voltage Droop control equation is modified as expressed in (3) by adding a non-linear decoupling term $\mathrm{J}_i(\mathrm{P}_{fi} - \mathrm{P}_{in})$, where J_i is expressed in (4) and depends on the measured voltage value E_{ref} at one of the studied mesh microgrid PCCs, acting as the pilot node. In our case we used the PCC called $\mu Gpcc$ (Fig. 1 and 2), through which the considered microgrid in Figure 2 can be connected to the main grid. The non-linear term $\mathrm{J}_i(\mathrm{P}_{fi} - \mathrm{P}_{in})$ allows removing the physical coupling between the active and reactive powers, caused by the voltage drop due to the power lines inductances and resistances. The estimation of J_i is performed using a simple integral controller, forcing an error ε_i defined in (5) to zero. Whatever the operating point and the active and reactive powers demanded by the loads, when the error ε_i tends to zero in steady state, an accurate reactive power sharing is achieved between the microgrid DGs.

$$\omega_i = \omega_{\mathrm{n}} - \mathrm{m}_i(\mathrm{P}_{fi} - \mathrm{P}_{in}) \tag{2}$$

$$E_i = E_{\mathrm{n}} - \mathrm{n}_i\left(\mathrm{Q}_{fi} - \mathrm{Q}_{in}\right) + \mathrm{J}_i(\mathrm{P}_{fi} - \mathrm{P}_{in}) \tag{3}$$

With:

$$\mathrm{J}_i = \mathrm{K}_I \int \varepsilon_i dt \tag{4}$$

$$\varepsilon_i = \left[\left(\frac{\mathrm{E}_{ref}}{E_n} - 1\right) + \left(\frac{\mathrm{Q}_{fi}}{\mathrm{Q}_{in}} - 1\right)\right] \tag{5}$$

And: $\begin{cases} \mathrm{m}_i = \frac{\Delta_\omega}{P_{in}} \\ \mathrm{n}_i = \frac{\Delta_E}{Q_{in}} \end{cases}$

It should be noted that E_{n} in (3) is the microgrid rated voltage. P_{in} and Q_{in} in (2), (3) and (5) are the rated values of the active and reactive powers of the i$^{\mathrm{th}}$ DG. P_i and Q_i as well as P_{fi} and Q_{fi} are respectively their measured and filtered values. ω_n and E_n are the rated values of the pulsation and voltage of the i$^{\mathrm{th}}$ DG. m_i and n_i are the droop control coefficients which are obtained using the permissible variations of DGs' pulsation Δ_ω and voltage Δ_E. It should be noted that the rated values of active and reactive powers of different DGs, used in their Droop-controllers, can be replaced by their available powers depending on the intermittency of their sources.

2.2. DGs' Synchronization in islanded mesh microgrids

Due to the intermittency of renewable energies, DGs' frequently connect to or disconnect from the microgrid. In order to achieve a fast and efficient synchronization of the i$^{\mathrm{th}}$ DG to the i$^{\mathrm{th}}$ PCC of the considered mesh microgrid, their voltage amplitudes E_i and E_{pcci}, their pulsations ω_i and ω_{pcci} as well as their phase angles ξ_i and ξ_{pcci} should be close enough. This is achieved by means of adding the terms $S1_i$ and $S2_i$ to the i$^{\mathrm{th}}$ DG Droop control equations as shown in (6) and (7). In these equations, the terms $S1_i$ and $S2_i$, containing the pure integral controllers, are multiplied by a binary coefficient called B_i, which is equal to one only during the synchronization interval and is set to zero otherwise. It should be noted that the synchronization procedure is presented in Figure 3.

$$\begin{cases} \omega_i = \omega_{\mathrm{n}} - \mathrm{m}_i\left(\mathrm{P}_{fi} - \mathrm{P}_{in}\right) - S1_i.\mathrm{B}_i \end{cases} \quad (6)$$

$$\begin{cases} E_i = E_{\mathrm{n}} - \mathrm{n}_i\left(\mathrm{Q}_{fi} - \mathrm{Q}_{in}\right) + \mathrm{J}_i\left(\mathrm{P}_{fi} - \mathrm{P}_{in}\right) - S2_{\mathrm{i}}.B_i \end{cases} \quad (7)$$

With:

$$\begin{cases} S1_i = \left[K_{ai}\int\left(\omega_i - \omega_{pcci}\right) + K_{bi}\int\left(\xi_i - \xi_{pcci}\right)\right] \\ S2_{\mathrm{i}} = \left[K_{ei}\int\left(E_i - E_{pcci}\right)\right] \end{cases}$$

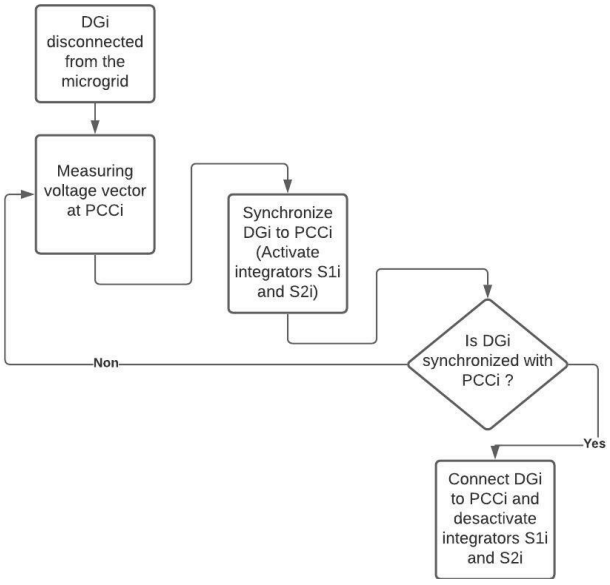

Fig.3. DGs' synchrinization procedure

2.3. Validation by simulation of the proposed power sharing and synchronization strategies in islanded mesh microgrids

In order to show the efficiency of the proposed control strategy for synchronization and power sharing in mesh microgrids with more than two DGs, the mesh microgrid of figure 1 is considered. The simulations are conducted using the Simscape toolbox of Matlab/Simulink. Each source, Source 1 (DG1), Source 2 (DG2) or source 3 (DG3), is modeled by a 3-phase voltage source controlled by E_{abcref_i} as presented in Figure 4. As shows Fig. 1, DG1, DG2 and

DG3 are connected respectively to PCC1, PCC2 and PCC6 (called also μ$Gpcc$). The equivalent synoptic diagram describing a droop-controlled DGi in Simscape is presented in Figure 5, in which it is shown how to determine E_{abcref_i} of the PCCi to which is connected the i[th] DG. This is done first by determining the voltage and current vectors (E_{dq_i} and I_{dq_i}) from the measured i[th] DG voltage and current vectors (E_{abc_i} and I_{abc_i}) by applying first the Concordia transformation $\boldsymbol{T}_{\mathbf{32}}^{\boldsymbol{t}}$, followed then by a rotation matrix $P(-\theta_i)$, as expressed in (8). It should be noted that θ_i is obtained by relation (9) using the pulsation ω_i expressed in (7), which is the output of the i[th] DG droop control. These vectors are used to calculate the active and reactive powers P_i and Q_i delivered by the i[th] DG as expressed in (10). The dynamics of the droop-control of i[th] DG are taken into account by adding a filter bloc in cascade with the power calculation bloc (Fig. 5).

$$\begin{cases} \begin{pmatrix} i_{di} \\ i_{q_i} \end{pmatrix} = P(-\theta_i).\boldsymbol{T}_{\mathbf{32}}^{\boldsymbol{t}} \begin{bmatrix} i_{ai} \\ i_{bi} \\ i_{ci} \end{bmatrix} = P(-\theta_i).\boldsymbol{T}_{\mathbf{32}}^{\boldsymbol{t}} \begin{bmatrix} i_{ai} \\ i_{bi} \\ -i_{ai} - i_{bi} \end{bmatrix} \\ \begin{pmatrix} E_{di} \\ E_{q_i} \end{pmatrix} = P(-\theta_i).\boldsymbol{T}_{\mathbf{32}}^{\boldsymbol{t}} \begin{bmatrix} v_{ai} \\ v_{bi} \\ v_{ci} \end{bmatrix} = P(-\theta_i).\boldsymbol{T}_{\mathbf{32}}^{\boldsymbol{t}} \begin{bmatrix} v_{aci} \\ v_{bci} \\ 0 \end{bmatrix} \\ \boldsymbol{T}_{\mathbf{32}}^{\boldsymbol{t}} = \sqrt{\frac{2}{3}} \begin{bmatrix} 1 & -\frac{1}{2} & -\frac{1}{2} \\ 0 & \frac{\sqrt{3}}{2} & -\frac{\sqrt{3}}{2} \end{bmatrix} \quad P(\theta) = \begin{bmatrix} \cos\theta & -\sin\theta \\ \sin\theta & \cos\theta \end{bmatrix} \end{cases} \tag{8}$$

$$\theta_i = \int \omega_i \, . \, dt \tag{9}$$

$$\begin{cases} P_i = E_{d_i} \, . \, i_{d_i} + E_{q_i} \, . \, i_{q_i} \\ Q_i = E_{q_i} \, . \, i_{d_i} - E_{d_i} \, . \, i_{q_i} \end{cases} \tag{10}$$

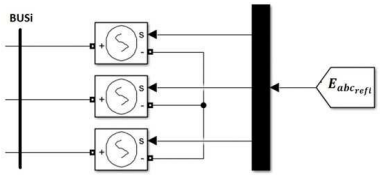

Fig.4. Controlable voltage source

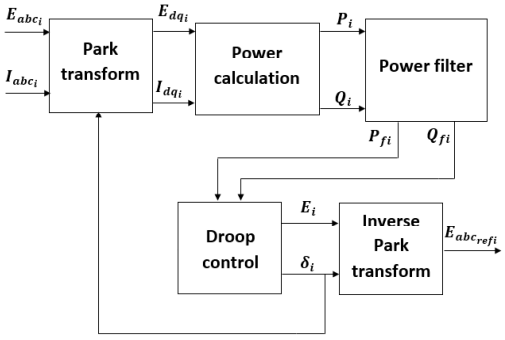

Fig.5. Equivalent synoptic diagram describing a droop-controlled DG in Simscape

For the performed simulations, the main microgrid parameters are listed in Table 1 and the rated powers of DGs and loads are listed in Table 2. To conduct the simulations, while applying the proposed control in (6) and (7), DG 1 imposes firstly the frequency and voltage of the microgrid and supplies load 1, 2 and 3 that are already connected to the microgrid up to t = 5 s. DG2 is synchronized during the interval 4 s to 5 s, and it is then connected to the microgrid at t = 5 s. At t = 10 s, the load 4 is connected to the microgrid. DG3 is synchronized during the interval 14 s to 15 s, and connected to the microgrid at t = 15 s. To verify the robustness of the proposed control method with respect to the load variations, the load 2 is disconnected at t = 20 s and reconnected at t = 25 s. Finally, to see the robustness of the

control with respect to topology changes, the Line 2-5 in Fig. 1 is disconnected at t = 30 s and reconnected at t = 35 s. The simulation results presented in figures 6a and 6b show that the proposed control in (6) and (7) ensures an accurate active and reactive power sharing in the considered islanded mesh microgrid under topology and load modification conditions, which proves its efficiency and its robustness. In addition, the proposed control strategy authorizes the DGs' smooth connection (synchronization) to the microgrid, which ensures the plug and play of the DGs and loads.

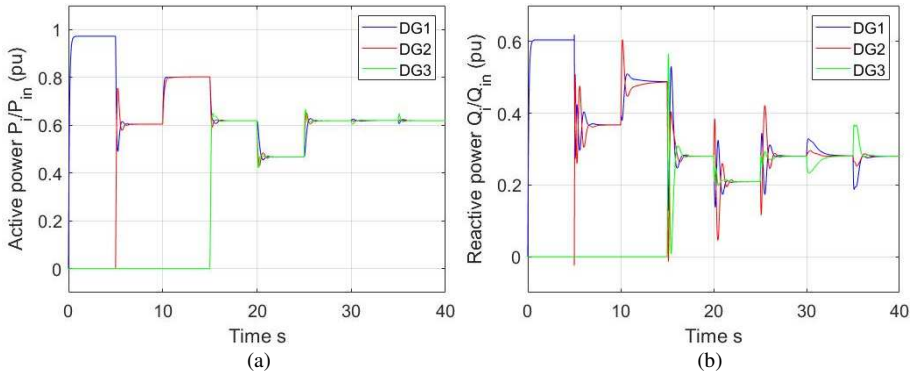

Fig.6. Evolution of the DGs' active (a) and reactive (b) powers (first DG supplies the microgrid up to 5 s, the second DG is connected to the microgrid at 5 s , the third DG is connected to the microgrid at 15 s)

2.4. Validation of the proposed control strategies in islanded mesh microgrids using HIL real time simulation

The efficiency of the proposed power sharing control strategy as well as the DGs' synchronization method is already verified by simulation results using Simscape of matlab/Simulink in the case of a 3-DG islanded mesh microgrid. In this section, the efficiency of the proposed power sharing control strategy as well as the DGs' synchronization methods are validated by experiments using Hardware in loop (HIL) real time simulations. The hardware in-the-loop (HIL) tests on the microgrid were conducted using two technologies. First Opal-RT with its NI PXIe-1072 system (Figure 7) is used to model the physical microgrid by a precise equivalent model that runs in real time. This NI PXIe-1072 system is equipped with digital inputs which are interfaced with the PMW outputs of the control system and DACs outputs connected to the ADCs inputs of the control system. The control system is developed in dSPACE technology via its Microlabbox (Figure 7). The 3-phases voltage generators are implemented in NI PXIe-1072 system thanks to 3-phases inverters with their LC output filters. Their control is implemented in the dSPACE system with a classical hierarchical control delivering the PWM signals presented in Figure 8 which are sent to the NI PXIe-1072 system. The cut-off frequency the voltage outer loops have been designed to be equal to 100 rad/s. The proposed power sharing strategy is implemented in the dSPACE system. The dynamics of VSI controllers have been taken into considerations for the HIL validations. Due to the limitation in the number of the ADCs inputs of the control system, the HIL validation of the proposed control strategies is performed using the mesh microgrid of Figure 2 having only two DGs in islanded operating mode. In addition, the robustness of the control with respect to extreme topology changes is also tested and validated using HIL. Figures 9a and 9b present the obtained results using HIL, showing the evolution of the active and reactive powers delivered by DG1 and DG2. DG1 imposes firstly the frequency and voltage of the 2-DG islanded mesh microgrid and supplies the loads up to t = 10 s. DG2 is synchronized with the voltage vector of the PCC2 during the interval 9 s to 10 s, and is connected to the microgrid at t = 10 s. It can be seen on Figures 9a and 9b that the DGs' synchronization strategy is efficient and their active and reactive power sharing are well ensured after the connection of DG2. In order to test and validate the robustness of the control with respect to microgrid topology modifications, a power line (line 2-5 in Fig. 2) is disconnected at t = 20 s and then reconnected at t = 30 s. It can be noticed that the active and reactive power sharing remains efficient even after the disconnection and reconnection of a power line.

Both the Simscape simulation results as well as the experimental HIL ones confirm the effectiveness of the non-linear control strategies in controlling the DGs' active and reactive power sharing of islanded mesh microgrids.

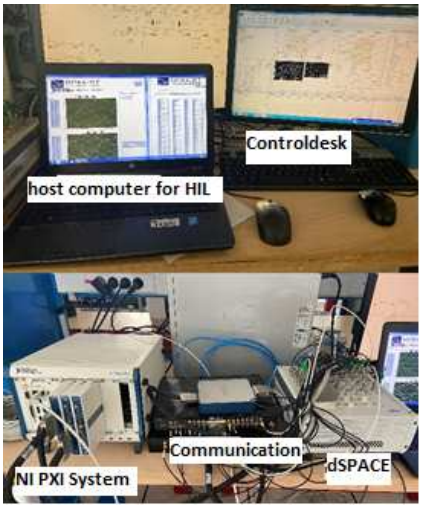

Fig.7. Experimental platform of the proposed HIL simulation system

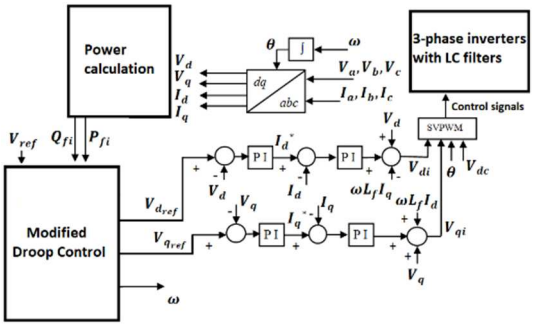

Fig.8. Hierarchical control of 3-phase voltage source inverter

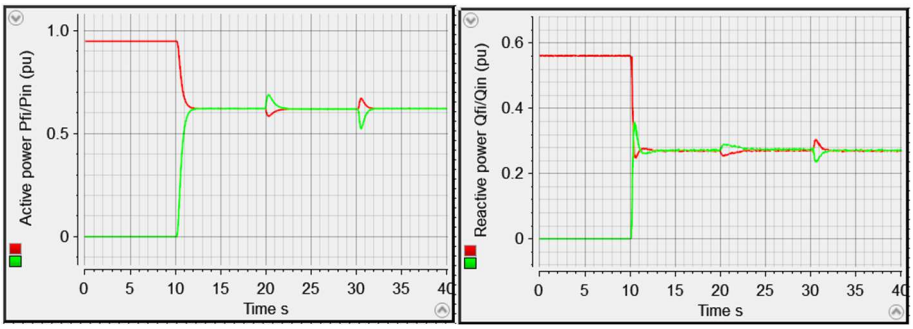

(a) (b)

Fig.9. Evolution of the DG active (a) and reactive (b) powers (first DG supplies the microgrid up to 10 s, the second DG is connected to the microgrid at 10 s. line 2-5 is disconnected at 20s then reconnected at 30 s)

3. DGs' Synchronization and Power Sharing in Mesh Microgrids in Islanded and Grid-connected modes

To synchronize the microgrids at a specific PCC called $\mu Gpcc$ to the main grid at a connection point called $Gridpcc$, the voltage vector at $\mu Gpcc$ should become almost equal to the voltage vector at $Gridpcc$. In other words their voltage amplitudes $E_{\mu Gpcc}$ and $E_{Gridpcc}$, their pulsations $\omega_{\mu Gpcc}$ and $\omega_{Gridpcc}$ as well as their phase angles $\xi_{\mu Gpcc}$ and $\xi_{Gridpcc}$ should become close enough. This is achieved by means of adding pure integral controllers to the DGs' Droop control equations of (6) and (7) already used in section 2 for islanded mesh microgrids. Then, the new control strategy for microgrids having the possibility to operate in both islanded and grid-connected modes is presented in (11) and (12). In these equations, the integral terms $S3_i$ and $S4_i$, for which the expressions are given in (13), act only during the

synchronization interval. At the interconnection instant these terms are fixed to their final values. In addition, to control the exchanged active power without affecting the exchanged reactive power after the connection of the microgrid to the main grid (grid-connected mode), the control strategy is improved by adding a new term ($Exch_P.D_i$) in the DGs' Droop-control equations (11). D_i is a binary coefficient which is equal to one in grid-connected mode and zero in islanded mode. The term $Exch_P$, for which the expressions are given in (13), allow forcing the active and reactive powers (P_{exch}) to its reference ($P_{exchref}$)

$$\begin{cases} \omega_i = \omega_0 - m_i(P_{fi} - P_{in}) - S1_i.B_i - S3_i + Exch_P.D_i & (11) \\ V_i = V_0 - n_i(Q_{fi} - Q_{in}) + J_i(P_{fi} - P_{in}) - S2_2.B_i - S4_i & (12) \end{cases}$$

With:

$$\begin{cases} S3_i = \left[K_{ai}\int(\omega_{\mu Gpcc} - \omega_{Gridpcc}) + K_{bi}\int\left(\xi_{\mu Gpcc} - \xi_{Gridpcc}\right)\right] \\ S4_i = [K_{ei}\int(E_{\mu Gpcc} - E_{Gridpcc})] \\ Exch_P = K_{I1}\int(P_{exchref} - P_{exch})dt \end{cases} \quad (13)$$

3.1. Simulation results in mesh microgrids in islanded and grid-connected modes

To test the efficiency of the proposed control mesh microgrids in both islanded and grid-connected operating modes, simulations are conducted using the Simscape toolbox of Matlab/Simulink on the considered mesh microgrid in figure 2 with 2 DGs and the main grid. Figures 10a and 10b demonstrate the evolution of the active and reactive powers delivered by DG1 and DG2. DG1 imposes firstly the frequency and voltage of the islanded mesh microgrid and supplies the loads up to t = 5 s. After the synchronization of the voltage vector of DG2 with the voltage vector of the PCC2 during the interval 4 s to 5 s, it is connected to the microgrid at t = 5 s. Then, during the interval [14s to 15s] the microgrid as a unit is synchronized with the main grid and connected at t = 15 s. During the interval [15s to 20s], the exchanged active power is controlled to be equal to zero by applying the aforementioned control strategy, expressed in (11) to (13). The reference $P_{exchref}$ of the absorbed exchanged active power from the main grid is set first to a positive value (2 kW) at t = 20 s. It is then set again to zero at t = 25 s. Finally, the absorbed exchanged active power reference $P_{exchref}$ is set to -2 kW at t = 30 s and -4 kW at t = 35 s to transfer a given positive active power to the main grid when it is possible.

It can be noticed that in figures 10a and 10b that the microgrid DGs' active and reactive power sharing in different operating modes is efficiently ensured, particularly during the synchronization interval (14 s<t<15 s) with the main grid and after their interconnection for $t \geq 15s$. In addition, there are no power peaks appearing after the connection of microgrid to the main Grid at t = 15 s. It can be also noticed that in figure 11a and 11b, between 15 s and 30 s, the exchanged active and reactive powers are maintained to zero, then the exchanged active power follows well its references as mentioned above. The exchanged reactive power changes during transitory states due to the DGs' voltage modifications, permitting to modify the exchanged active power with the main grid.

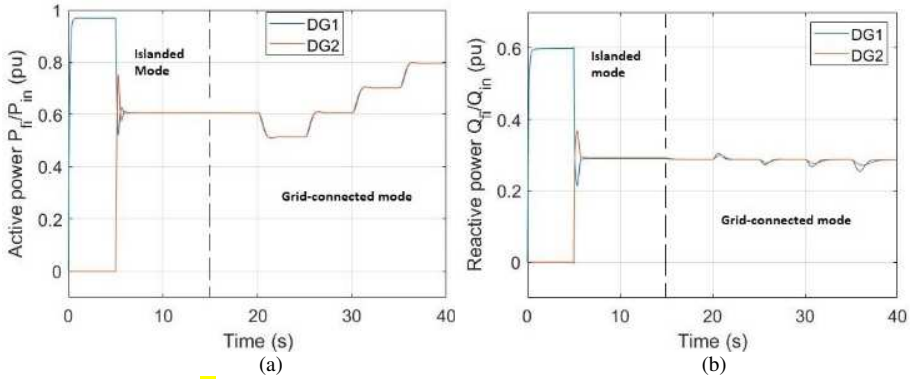

Fig.10. Evolution of the DGs' active (a) and reactive (b) powers (first DG supplies the islanded microgrid up to 5 s, the second DG is connected to the microgrid at 5 s and the interconnection between the microgrid and the main grid takes place at 15 s)

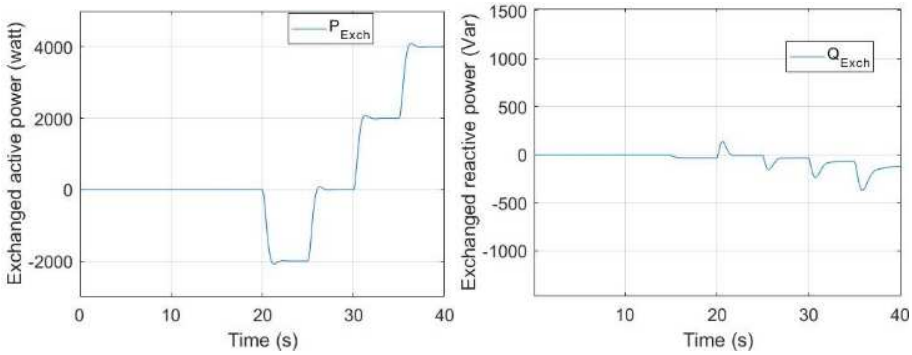

(b) (b)

Fig.11. Evolution of the exchanged active (a) and reactive (b) powers between the microgrid and the main grid.

Remarque: In islanded mode, with the proposed control strategy in this paper, as the DGs in the considered microgrid act like grid-forming units and their controllers impose their frequencies and voltages, the DGs' power is not then imposed directly. This point can be limiting for small scale DGs as they should compete with larger scale ones. While in grid connected mode, this problem stops to exist because usually the DGs work in grid-following mode. Thus, the microgrid voltage and frequency are imposed by the main grid. In this case, in order to not limit small scale DGs, the power of a small-scale DG can be increased to the maximum/rated output value and be kept constant while other DGs adapt their output if needed. A global energy management system has to be implemented at secondary or tertiary level. For our application, the DGs still operate in grid-forming mode after connection to the main grid. If such an objective has to be achieved, the tertiary proposed strategy has to be changed to take into account these new constraints. This point is not treated in this paper.

3.2. Validation using hardware-in-the-loop simulation in grid-connected mode

In order to validate the proposed strategies for microgrid synchronization, and power exchange control in grid-connected mode using real-time HIL simulations. The same simulation scenarios that was adopted in section 2 is applied here. Figures 12a and 12b show the evolution of active and reactive powers of the two DGs connected to the microgrid. DG1 imposes firstly the frequency and voltage of the two-DGs islanded mesh microgrid and supplies the loads up to t = 10 s. DG2 is synchronized with the voltage vector of the PCC2 during the interval 9 s to 10 s, and is connected to the microgrid at t = 10 s. After the connection of the second DG (DG2) at t = 10 s, the synchronization of the microgrid as a unit with the main grid is performed and then they are connected at t = 20 s. The exchanged power control strategy is performed to maintain the exchanged active power to 0 during the period [20s-30s]. By changing $P_{exchref}$, at t = 30 s a positive active power of 2 kW from the main grid is demanded, then at t = 40 s the demanded active power is set again to 0. Finally, $P_{exchref}$ is set to -2 kW at t = 50 s and -4 kW at t = 60 s to transfer positive active powers to the main grid when the microgrid DGs are capable to produce more than the power required by its loads. It can be noticed that in figure 12a and 12b the active and reactive power-sharing is well ensured during the synchronization interval (10 s<t<20 s) and after the interconnection for t$\geqslant$ 20 s. In addition, there are no power peaks appearing after the connection of microgrid to the main Grid at t = 20 s. It can be also noticed that in figure 13a and 13b between 20 s and 30 s the exchanged active and reactive powers are maintained to zero, then they follow well their references as mentioned above. The exchanged reactive power changes a little bit during transitory states due to the changes in $P_{exchref}$ but it returns to a weak value in steady-state.

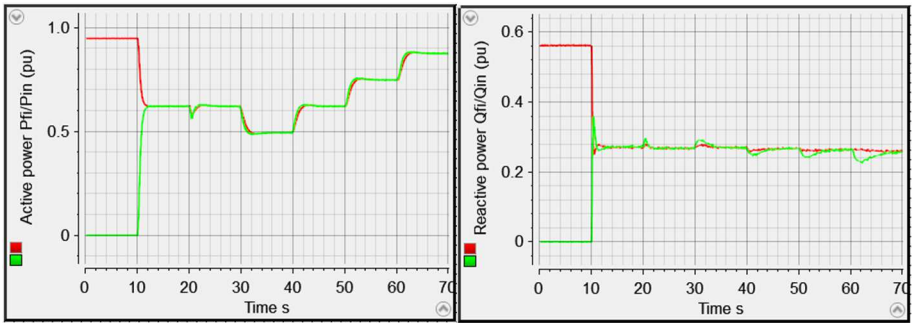

(a) (b)

Fig.12. Evolution of the DGs' active (a) and reactive (b) powers (first DG supplies the microgrid up to 10 s, the second DG is connected to the microgrid at 10 s and the interconnection between the microgrid and the main grid takes place at 20 s)

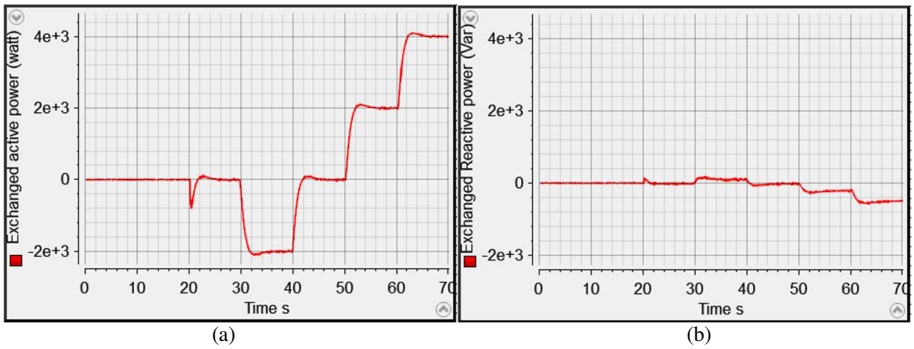

(a) (b)

Fig.13. Evolution of the exchanged active (a) and reactive (b) powers between the microgrid and the main grid.

3.3. Rrobustness study of Mesh microgrid control in islanded and grid connected operating modes

Based on the mesh microgrid model established in NI PXIe-1072, including the proposed nonlinear control established in dSPACE, the control robustness of the considered mesh microgrid (Fig. 2) with respect to large load variations and sudden changes in topology is studied in islanded and grid connected operating modes. In both modes, two robustness tests are applied. The first test is disconnecting and then reconnecting a random line in the microgrid leading to a topology modification. The second test is the application of a large load variation to the microgrid by disconnecting a load in the microgrid followed by its reconnection.

In islanded mode, after the connection of DG1 and DG2 at respectively t = 0 s and t = 20 s, line 1-4 (Fig. 2) is disconnected at t = 40 s and then reconnected at t = 60 s. Subsequently, the load 3 is disconnected at t = 80 s and reconnected at t = 100 s.

In grid-connected mode, the interconnection between the microgrid and the main grid takes place at 120s. The exchanged power control strategy is performed to maintain the exchanged active power to 0 during the period [120s-140s]. By changing $P_{exchref}$, at t = 140 s a positive active power of 2 kW is transferred to the main grid. To observe the effect of the topology changes on control in grid-connected mode, line 2-5 is disconnected at t = 160 s and then reconnected at t = 190 s. Finally, to verify the effect of large load variation on the control of the grid connected microgrid, the load 2 is disconnected at t = 220 s and then reconnected at t = 250 s.

It can be noticed in figures 14a and 14b that in both islanded and grid connected operating modes, the active and reactive power sharing remains ensured after the changes in the mesh microgrid topology and also during large load variations. It can also be noticed in figures 15a and 15b that in grid-connected operating mode those tests didn't affect the exchanged active and reactive powers in steady state. The effectiveness of the proposed control strategy to allow plug and play functionality of DGs and loads while ensuring accurate sharing of active and reactive powers, even if the microgrid topology is dynamically modified, confirms its robustness.

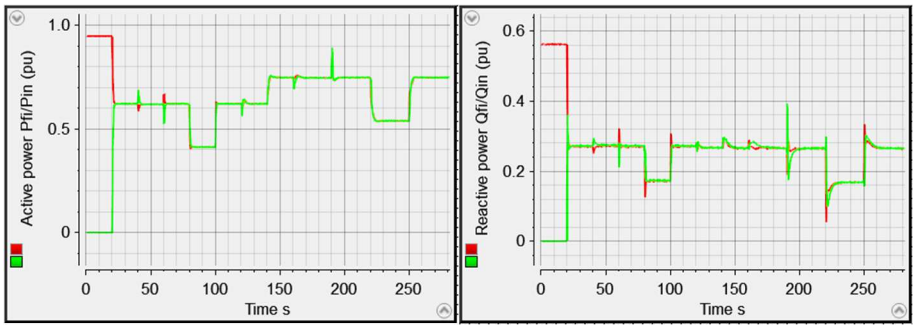

(a) (b)

Fig.14. Evolution of the DG's active (a) and reactive (b) powers (first DG supplies the microgrid up to 20 s, the second DG is connected to the microgrid at 120 s and the interconnection between the microgrid and the main grid takes place at 20 s)

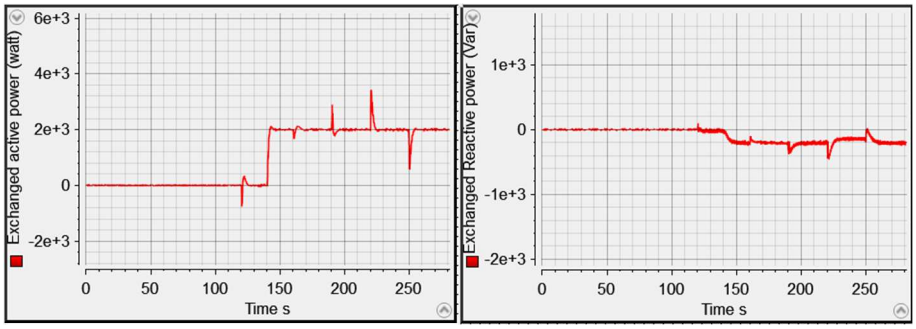

(a) (b)

Fig.15. Evolution of the exchanged active (a) and reactive (b) powers between the microgrid and the main grid.

4. Communication delay impact on microgrid stability in islanded mode

The proposed control for power sharing in islanded operation mode is distributed and uses the information on the measured RMS value of the voltage at a pilot node (the node µGpcc in Fig. 16) which is sent to all the microgrid DGs local controllers. The access to this information necessitates a one-way communication from the node µGpcc to all the connected DGs to the microgrid as shown in Figure 16. This communication can affect the microgrid stability if important communication delays occur [22]-[23].

In order to examine and evaluate the impact of the communication delay on the proposed nonlinear control, the mesh microgrid of Figure 1, where all of the 3 DGs are connected to the islanded microgrid at t = 0 s, is modeled using MATLAB/Simscape. First, the conventional droop control (without the non-linear term $J_i(P_{fi} - P_{in})$ in (3)) is applied up to t = 5 s. At t = 5 s the proposed nonlinear control for power sharing is applied by adding the nonlinear term $J_i(P_{fi} - P_{in})$ in (3). As mentioned above, this term needs to receive the information on the RMS value of the µGpcc voltage as shown in Figure 17. To consider the communication time delay for receiving this information, a first order filter with a time constant of T_d , for which the expression is detailed in equation (14), is added to the MATLAB/Simscape scheme (Figure 17). To investigate the impact of the communication time delay on the efficiency of the proposed power sharing control method and the microgrid stability the value of T_d is modified from 300 ms to 1.7 s. Then at 15 s load 2 is disconnected to test the robustness of the control with respect to load variation while applying communication delays.

$$\frac{E^*_{ref}}{E_{ref}} = \frac{1}{1+\frac{1}{T_d}*s} \qquad (14)$$

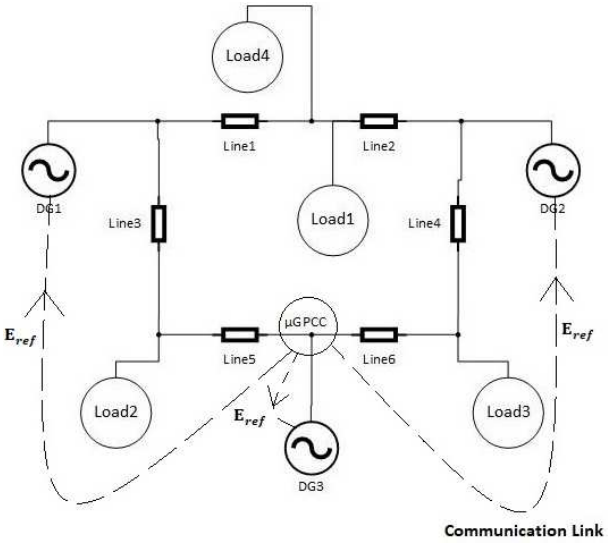

Fig.16. 3-DG microgrid

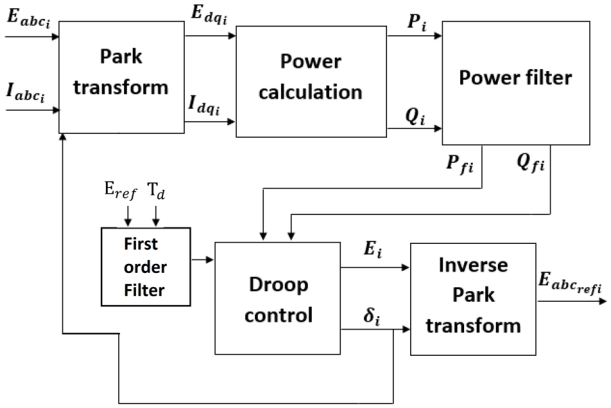

Fig.17. Equivalent synoptic diagram describing a droop-controlled DG in Simscape

For the first communication delay test, figures 18a and 18b show the evolution of DGs' active and reactive powers when the communication delay is set to 300 ms which represent the slowest wide range communication technology [23]. It can be seen that the active and reactive power sharing is not affected and the microgrid stability remains ensured even after the disconnection of load 2 at 15 s. When the communication delay is set to 600 ms, the controller performance seems to be slightly affected. Oscillations can be observed on DGs' active and reactive powers after the application of the nonlinear control at 5 s and after the disconnection of load 2 at 15 s. However, these power oscillations attenuate and the DGs' accurate power sharing is regained as presented in figures 19a and 19b. Finally, when the communication delay is set to 1.7 s the power sharing is totally lost and microgrid becomes instable, as presented in figures 20a and 20b. In more details, the high communication delay, results in calculation errors for nonlinear term. Moreover, the droop controller cannot accurately calculate the droop correction terms.

The maximum communication delay that can be handled by the controller is 1.4 s which translate to a way slower communication than any wide range communication technology available. This result means that the proposed control strategy is robust enough against practical values of the communication delay and consequently can be applied to the control of mesh microgrids' DGs.

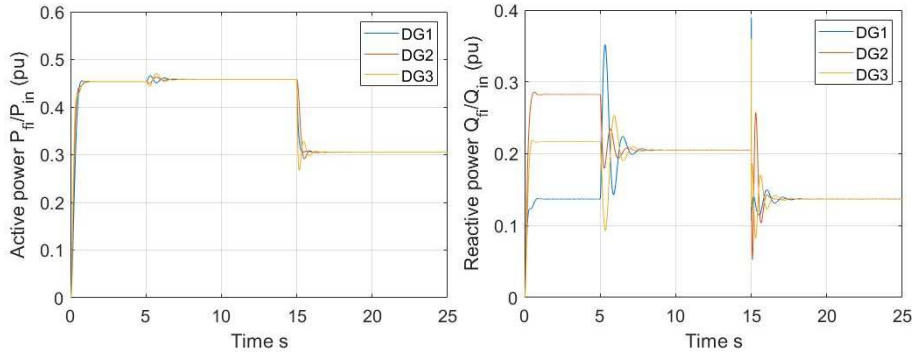

(a) (b)

Fig.18. Evolution of the DGs' active (a) and reactive (b) powers with a communication delay of 300 ms (All DGs are connected to the microgrid at 0 s. Load 2 is disconnected at 15 s).

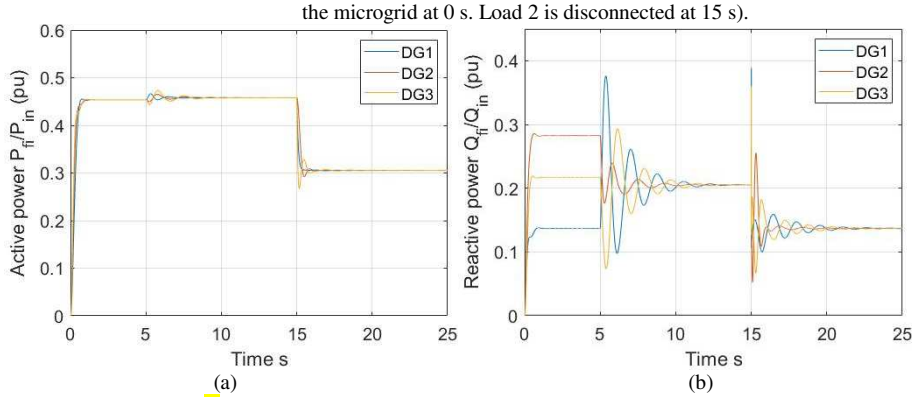

(a) (b)

Fig.19. Evolution of the DGs' active (a) and reactive (b) powers with a communication delay of 600 ms (All DGs are connected to the microgrid at 0 s. Load 2 is disconnected at 15 s).

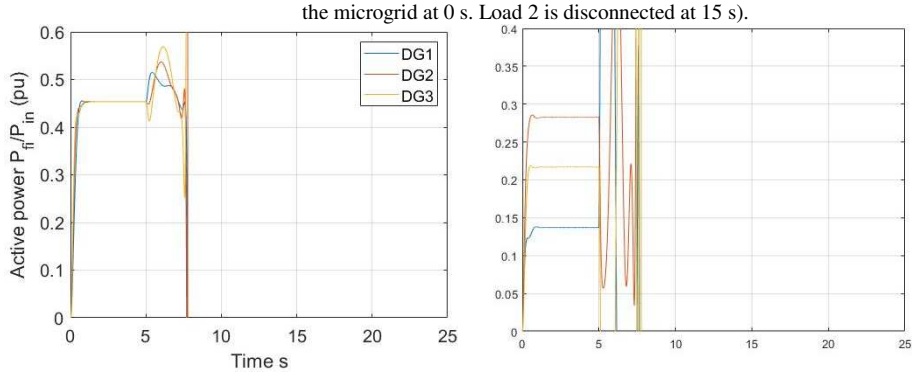

(a) (b)

Fig.20. Evolution of the DGs' active (a) and reactive (b) powers with a communication delay of 1.7 s (All DGs are connected to the microgrid at 0 s).

5. Conclusion

A novel nonlinear control strategy for synchronization and power sharing in islanded or grid-connected mesh microgrids is investigated. It allows the synchronization of DGs to the microgrid, as well as the microgrid as a unit to the main-grid, while ensuring DGs' active and reactive power sharing and the possibility to control independently the exchanged active and reactive powers with the main grid in grid-connected mode. The different simulation tests proved the efficiency of the proposed control strategy for fast synchronization as well as DGs' active and reactive power sharing and a robust control of the exchanged power with the main grid. In order to validate the proposed control strategy safely, hardware in the loop HIL tests are conducted. The HIL tests were carried using Opal-RT via

NI PXI system and dSPACE technologies. By using HIL simulation, all the proposed strategies are proved to be efficient. The robustness of the proposed control strategy with respect to sudden topology and load modifications are successfully verified by applying the line power and load disconnection and reconnection tests to the considered mesh microgrid in both islanded and grid-connected operating modes. As well, the nonlinear term added to the conventional Droop control allows ensuring efficient active and reactive power sharing in both islanded and grid-connected operating modes. The only information required to apply the proposed control strategy is the measured voltage and current vectors in a pilot PCC, through which the microgrid can be connected to the main grid creating a one-way communication. Several tests considering various values of the communication time delay are conducted to evaluate its impact on the performances of the proposed control strategy. The obtained results highlighted that the proposed control strategy is enough robust against communication delay to be practically applied to the control of mesh microgrids' DGs.

To summarize, the main contributions of the proposed control of mesh microgrids in this paper concerns the following aspects.

- The proposed control strategy ensures an accurate power sharing while providing the "plug and play" function in both islanded and grid connected operating modes.
- It ensures a seamless transition from islanded to grid connected modes of mesh microgrids without affecting the DGs' active and reactive power sharing during the synchronization phase.
- In grid-connected mode, the proposed control allows the exchange of active power between the microgrid and the main grid without affecting the DGs' active and reactive power sharing.
- In both operating modes of mesh microgrids, the control is robust with respect to large load variations and microgrid topology changes.
- The proposed control is robust with respect to high communication delays and can be used in practice.

Acknowledgements

This project was financially supported by Ministry of Europe and Foreign Affairs, Ministry of Higher Education, Research and Innovation and the French Institute of Rabat (PHC TOUBKAL 2019 (French–Morocco bilateral program) Grant Number: 12345AB).

References

[1] T. V. Hoang and H. Lee, "An Adaptive Virtual Impedance Control Scheme to Eliminate the Reactive-Power-Sharing Errors in an Islanding Meshed Microgrid," in IEEE Journal of Emerging and Selected Topics in Power Electronics, vol. 6, no. 2, pp. 966-976, June 2018.

[2] A. Mehrizi-Sani and R. Iravani, "Adaptive droop control applied to voltage-source inverters operating in grid-connected and islanded modes," IEEE Trans. Ind. Electron., vol. 56, no. 10, pp. 4088 - 4096, Oct. 2009.

[3] A. Mehrizi-Sani and R. Iravani, "Mode adaptive droop control with virtual output impedances for an inverter-based flexible Ac microgrid," IEEE Trans. Power Electron., vol. 26, no. 3, pp. 689 - 701, March 2011.

[4] K. De Brabandere, B. Bolsens, J. Van den Keybus, A. Woyte, J. Driesen, and R. Belmans, "A voltage and frequency droop control method for parallel inverters," IEEE Trans. Power Electron., vol. 22, no. 4, pp. 1390 - 1420, Apr. 2007.

[5] R. Moslemi, J. Mohammadpour and A. Mesbahi, "A modified droop control for reactive power sharing in large microgrids with meshed topology," *2016 American Control Conference (ACC)*, 2016.

[6] C. N. Papadimitriou, E. I. Zountouridou, and N. D. Hatziargyriou. "Review of hierarchical control in DC microgrids." Electr. Power Syst. Res. Vol. 122, pp. 159-167, 2015.

[7] T. Dragičević, X. Lu, J. C. Vasquez and J. M. Guerrero, "DC Microgrids—Part I: A Review of Control Strategies and Stabilization Techniques," IEEE Trans. Power Electron., vol. 31, no. 7, pp. 4876- 4891, July 2016.

[8] F. Nejabatkhah and Y. W. Li, "Overview of Power Management Strategies of Hybrid AC/DC Microgrid," IEEE Trans. Power Electron., vol. 30, no. 12, pp. 7072-7089, Dec. 2015.

[9] J. Jiao, S. Guo, C. Tan, Y. Xue and X. Hua, "Research on Improved Droop Control Method of DC Microgrid Based on Voltage Compensation," *2020 5th International Conference on Power and Renewable Energy (ICPRE)*, Shanghai, China, 2020, pp. 391-395.

[10] H. Mahmood, D. Michaelson and J. Jiang, "Accurate Reactive Power Sharing in an Islanded Microgrid Using Adaptive Virtual Impedances," in *IEEE Transactions on Power Electronics*, vol. 30, no. 3, pp. 1605-1617, March 2015.

[11] J. He, Y. Pan, B. Liang and C. Wang, "A Simple Decentralized Islanding Microgrid Power Sharing Method Without Using Droop Control," in IEEE Transactions on Smart Grid, vol. 9, no. 6, pp. 6128-6139, Nov. 2018.

[12] H. Moussa, A. Shahin, J. Martin, S. Pierfederici and N. Moubayed, "Optimal Angle Droop for Power Sharing Enhancement With Stability Improvement in Islanded Microgrids," in IEEE Transactions on Smart Grid, vol. 9, no. 5, pp. 5014-5026, Sept. 2018.

[13] Chia-Tse Lee, Chia-Chi Chu and Po-Tai Cheng, "A new droop control method for the autonomous operation of distributed energy resource interface converters," IEEE Trans. Power Electron., vol. 28, no. 4, pp. 1980 - 1993, Apr. 2013.

[14] D. K. Dheer, O. V. Kulkarni, S. Doolla and A. K. Rathore, "Effect of Reconfiguration and Meshed Networks on the Small-Signal Stability Margin of Droop-Based Islanded Microgrids," in *IEEE Transactions on Industry Applications*, vol. 54, no. 3, pp. 2821-2833, May-June 2018.

[15] Y. Zhu, B. Liu, F. Wang, F. Zhuo, and Y. Zhao, "A virtual resistance based reactive power sharing for networked microgrid," in proc. 9th international conference on power electron., Seoul, Korea, 2015, pp. 1430 - 1441.

[16] Y. Zhu, F. Zhuo, F. Wang, B. Liu, R. Gou and Y. Zhao, "A Virtual Impedance Optimization Method for Reactive Power Sharing in Networked Microgrid," in *IEEE Transactions on Power Electronics*, vol. 31, no. 4, pp. 2890-2904, April 2016.

[17] Y. Hennane, A. Berdai, J.-P. Martin, S. Pierfederici, and F. Meibody-Tabar, "New Decentralized Control of Mesh AC Microgrids: Study, Stability, and Robustness Analysis," *Sustainability*, vol. 13, no. 4, p. 2243, Feb. 2021.

[18] C. Lee, R. Jiang and P. Cheng, "A Grid Synchronization Method for Droop-Controlled Distributed Energy Resource Converters," in IEEE Transactions on Industry Applications, vol. 49, no. 2, pp. 954-962, March-April 2013.

[19] X. Haizhen, Z. Xing, L. Fang, Z. Debin, S. Rongliang, N. Hua, and C.Wei, "Synchronization strategy of microgrid from islanded to grid-connected mode seamless transfer," presented at IEEE International Conference of IEEE Region 10 (TENCON 2013), 2013.

[20] S. Paghdar, U. Sipai, K. Ambasana and P. J. Chauhan, "Active and reactive power control of grid connected distributed generation system," 2017 Second International Conference on Electrical, Computer and Communication Technologies (ICECCT), 2017.

[21] K.-L. Nguyen, D.-J. Won, S.-J. Ahn, and I.-Y. Chung, "Power Sharing Method for a Grid connected Microgrid with Multiple Distributed Generators," *Journal of Electrical Engineering and Technology*, vol. 7, no. 4. The Korean Institute of Electrical Engineers, pp. 459–467, 01-Jul-2012.

[22] D. Baros, N. Rigogiannis, N. Papanikolaou and M. Loupis, "Investigation of Communication Delay Impact on DC Microgrids with Adaptive Droop Control," *2020 International Symposium on Industrial Electronics and Applications (INDEL)*, 2020, pp. 1-6

[23] M. Saleh, Y. Esa, A. Mohamed, "Impact of Communication Latency on the Bus Voltage of Centrally Controlled DC Microgrids During Islanding," IEEE Trans. Sust. Energy, vol. 10, no. 4, pp. 1844–1856, Oct. 2019.